Applied Physics Letters

Terahertz photoconductance dynamics of semiconductors from sub-nanosecond to millisecond timescales

Cite as: Appl. Phys. Lett. **122**, 012101 (2023); https://doi.org/10.1063/5.0130721
Submitted: 14 October 2022 • Accepted: 17 December 2022 • Published Online: 03 January 2023

Edward Butler-Caddle, Nicholas E. Grant, Sophie L. Pain, et al.

Applied Physics Letters ARTICLE scitation.org/journal/apl

Terahertz photoconductance dynamics of semiconductors from sub-nanosecond to millisecond timescales

Cite as: Appl. Phys. Lett. **122**, 012101 (2023); doi: 10.1063/5.0130721
Submitted: 14 October 2022 · Accepted: 17 December 2022 ·
Published Online: 3 January 2023

Edward Butler-Caddle,[1,a)] Nicholas E. Grant,[2] Sophie L. Pain,[2] John D. Murphy,[2] K. D. G. Imalka Jayawardena,[3] and James Lloyd-Hughes[1,a)]

AFFILIATIONS

[1]Department of Physics, University of Warwick, Coventry CV4 7AL, United Kingdom
[2]School of Engineering, University of Warwick, Coventry CV4 7AL, United Kingdom
[3]Advanced Technology Institute, Department of Electrical and Electronic Engineering, University of Surrey, Guildford, Surrey GU2 7XH, United Kingdom

[a)]**Authors to whom correspondence should be addressed:** E.Butler-Caddle@warwick.ac.uk and J.Lloyd-Hughes@warwick.ac.uk

ABSTRACT

Optical pump terahertz probe spectroscopy (OPTP) is a versatile non-contact technique that measures transient photoconductance decays with femtosecond temporal resolution. However, its maximum temporal range is limited to only a few nanoseconds by the mechanical delay lines used. We extended the temporal range of OPTP to milliseconds and longer while retaining sub-nanosecond resolution. A separate pump laser was electrically synchronized to the probe pulses, allowing the pump–probe delay to be controlled with an electronic delay generator. We demonstrated the capabilities of this technique by examining the photoconductance decays of semiconductors with lifetimes ranging over six orders of magnitude: III-Vs, metal halide perovskites, germanium, and silicon. A direct comparison of results on silicon from OPTP and inductively coupled photoconductance decay highlighted the higher spatial and temporal resolution of OPTP, which allowed in-plane and out-of-plane carrier diffusion to be studied.

The transient photoconductance decay of a material after pulsed photoexcitation gives valuable information about charge carrier mobilities and recombination lifetimes, which are critical properties for electronic device performance. Optical pump terahertz probe spectroscopy (OPTP) is a non-contact technique in which the transient photoconductance is sampled by measuring the transmission (or reflection) of a single-cycle pulse of free space THz radiation.[1–3] Other techniques that measure photoconductance decays in a non-contact manner include time resolved microwave conductivity (TRMC),[4–7] which measures the transmission (or reflection) of a continuous wave AC electric field at GHz frequencies, and inductively coupled photoconductance decay (PCD),[8–10] which induces and measures eddy currents at radio frequencies. Since these techniques probe at different frequencies, the properties that they measure may differ as both the conductivity response of a material and the penetration depth of the probing field are a function of frequency.[10,11] OPTP has the highest spatial resolution, with diffraction-limited spot sizes around 1 mm, whereas TRMC and PCD setups probe areas with dimensions of centimeters. Probing smaller areas is particularly beneficial for sample mapping[12] and to study the in-plane diffusion of carriers, as will be demonstrated in this work. OPTP also has the best time resolution (down to tens of fs), in comparison to the typically ns and μs resolution of TRMC and PCD, respectively.

In a typical OPTP setup, both the pump and probe pulses are derived from the same femtosecond laser using a beam splitter, and the pump–probe delay can be varied with femtosecond precision by changing the path length of one of the beams. However, mechanical delay lines are challenging to align, and the maximum pump–probe delay achievable is only a few nanoseconds. Hence, for samples with effective lifetimes longer than a few hundred picoseconds, only the earliest part of the decay can be measured, and discriminating between alternative recombination pathways becomes challenging.[13]

In this work, in order to probe photoconductance decays via OPTP over longer time ranges, we used a separate, electronically triggered laser to generate the pump beam. The femtosecond master laser generated an electronic signal that was synchronized to its optical

emission and was sent to the pump laser via a delay generator, allowing the pump–probe delay to be varied. Similar electronically delayed OPTP spectroscopy methods, hereafter named E-OPTP, have been reported previously.[14,15] In a scheme that generated THz radiation using a laser oscillator,[14] the probe was a series of consecutive THz pulses lasting 95 ns, limiting the temporal resolution, while the pump–probe delay range was limited to 200 μs. E-OPTP was used to examine photoconductance decays in metal halide perovskites over a time range of ~100 ns.[15] Here, we demonstrate E-OPTP with a wide temporal range (10 ms) and excellent time resolution (~200 ps) in a study of semiconductors with different recombination lifetimes. Furthermore, we highlight the factors limiting temporal resolution in E-OPTP and describe a method for efficiently measuring photoconductance decays that exceed the repetition period of the probe, allowing a comparison with PCD for results on passivated silicon. The high spatial and temporal resolution, and wide time window of E-OPTP allowed features in the photoconductance decay curves to be linked to in-plane and out-of-plane diffusion via analytical solutions of the (spatially dependent) continuity equations.

THz pulses were generated using an amplified Ti:Sapphire laser (Spectra Physics Spitfire) and a spintronic THz emitter[16] and detected via electro-optic sampling in a (110) ZnTe crystal. E-OPTP was implemented with two alternative lasers: a fiber-based master oscillator power amplifier (MOPA) laser from Ikeos Research, with a center wavelength of 1550 nm and a pulse duration of ~200 ps; and a pulsed laser diode (Thorlabs NPL45C), with a center wavelength of 450 nm, a variable pulse duration of 6–129 ns, and an approximately square temporal profile. Electrical delay was provided by a commercial delay generator: either a Quantum Composers (QC) 9530 or a Stanford Research Systems (SRS) DG645.

The pump-induced fractional change in THz transmission, $\Delta T/T$, is related to the pump-induced change in the dielectric response of the sample.[1,3] In this work, $\Delta T/T$ was measured via electro-optic sampling, using a precision oscilloscope to record the balanced photodiode outputs for four consecutive gate pulses, labeled A, B, C, and D, as shown in Fig. 1(a). The THz electric field with the pump beam incident on the sample, E_{on}, was determined from $E_{on} \propto A - B$, while E_{off}, the transmitted THz field strength without the pump beam, was given by $E_{off} \propto C - D$. In contrast to double-demodulation based on lock-in amplifiers,[3] sampling $\Delta T/T$ via an oscilloscope permits a shot-by-shot analysis of the statistics (e.g., standard deviation; median) of the dataset. $\Delta T/T$ was calculated from

$$\frac{\Delta T}{T} \equiv \frac{E_{on} - E_{off}}{E_{off}} = \frac{(A - B) - (C - D)}{C - D}. \quad (1)$$

In the limit of small $\Delta T/T$, adopted herein, the sheet photoconductance is $\Delta\sigma \propto -\Delta T/T$.[17]

Figure 1(b) reports $\Delta T/T$ transients obtained on a variety of indirect and direct bandgap semiconductors, which could not have been measured using a mechanical delay line. An unpassivated n-type Ge wafer ($n_0 \leq 10^{14}$ cm^{-3}) and InSb or InAs epitaxial layers were excited with the 1550 nm laser, while a passivated Si wafer and a film of the triple cation lead-halide perovskite[18,19] $Cs_{0.05}(FA_{0.83}MA_{0.17})_{0.95}Pb(I_{0.83}Br_{0.17})_3$ were excited with the 450 nm laser. The InAs, InSb, and perovskite were fitted with monoexponential decays (dashed lines), yielding lifetimes of 1, 6, and 170 ns, respectively. For Ge, $\Delta T/T$ had a faster decay over the first few hundred nanoseconds, followed by a slower monoexponential decay (20 μs lifetime) commensurate with its indirect bandgap and low trap density, and consistent with lifetimes from TRMC.[20] Results for Si are discussed later.

We now highlight the factors that affect the precision and accuracy of the temporal resolution in E-OPTP. In both electronic and mechanical delay schemes, the ultimate temporal resolution of the probe for a single shot is set by the response function of electro-optic sampling, i.e., the optical gate pulse duration (40 fs) and response of the non-linear crystal.[21] However, the temporal resolution is poorer for E-OPTP than for mechanical delay: the minimum delay step is greater (5 ps here), and the pump–probe delay jitter (shot-to-shot fluctuations in delay time) is larger. Jitter broadens the temporal response function for the mean of multiple repeats compared to the response function for a single shot. We assessed the jitter for each component using an oscilloscope to measure the distribution of pulse arrival times relative to the input signal. It was found that the QC 9530 delay generator had a peak-to-peak jitter of 2.4 ns, whereas the SRS DG645 delay generator and all other components had jitters smaller than 0.4 ns.

The impact of timing jitter in E-OPTP was further quantified using the histograms and statistics for 200 samples of $\Delta T/T$ for the photoconductance rise of a Ge wafer pumped with the 1550 nm laser, as shown in Fig. 2 (brighter purple representing more counts). For the QC 9530 delay generator [Fig. 2(a)], the temporal resolution, as assessed from the duration of the rise in signal, was dominated by the

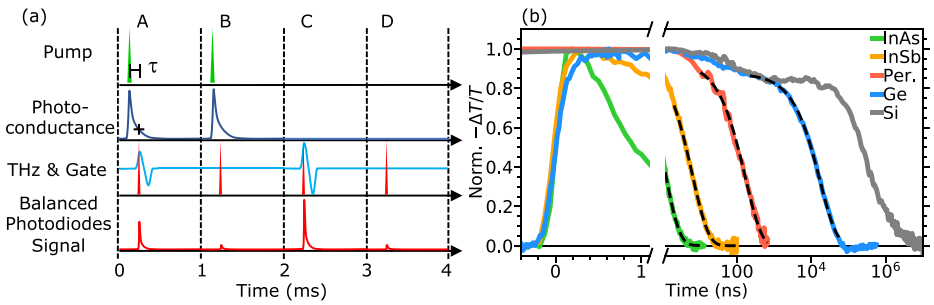

FIG. 1. (a) E-OPTP double modulation scheme (see the text) used to sample the photoconductance $\Delta\sigma \propto -\Delta T/T$ at pump–probe decay τ, indicated by the cross. The THz pulse is shown expanded in time for clarity. (b) Normalized photoconductance decays for Ge, InSb, and InAs excited by the 1550 nm laser, and a lead-halide perovskite (Per.) film or a passivated Si wafer excited by the 450 nm laser. Single-exponential fits are indicated by dashed lines. All curves were acquired with the pulse scheme in panel (a), except for the data on Si, which required the "extended mode" scheme discussed with regard to Fig. 3.

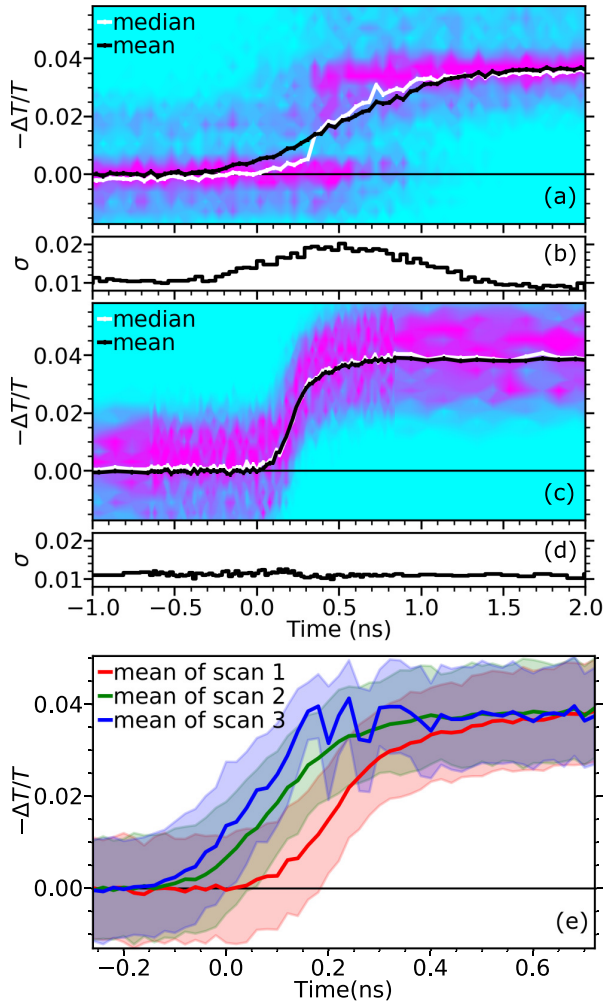

FIG. 2. (a) 2D histogram of 200 repeat measurements of $\Delta T/T$ for Ge wafer excited at 1550 nm, plotted against nominal pump–probe delay set using the QC 9530 delay generator. Purple indicates more counts, while cyan represents zero counts. (b) Standard deviation, σ, of $\Delta T/T$ from (a). Panels (c) and (d) are same as (a) and (b) but using the SRS DG645 delay generator. (e) The mean (lines) and standard deviation (shaded) of $\Delta T/T$ obtained from 200 repeat measurements at each pump–probe delay, for three different sweeps (scans 1–3) over the delay range, taken at 5 min intervals. Scan 1 data also shown in (c) and (d) (Ge wafer; 1550 nm excitation; SRS DG645 delay generator).

2.4 ns jitter of the delay generator. Near the rapid change in $\Delta T/T$ at zero pump–probe delay [around 0.5 ns in panel (a)], temporal jitter created a bimodal distribution and added noise to $\Delta T/T$, evident by the increase in its standard deviation σ [Fig. 2(b)]. The smaller jitter of the SRS DG645 resulted in a unimodal distribution and an improved temporal resolution [panel (c)], and a noise independent of pump–probe delay [panel (d)]. The SRS DG645's timing jitter increases linearly as a function of delay time at a rate of 10^{-8} s/s from a minimum of 20–30 ps and, hence, would only reach 130 ps even with electronic delays of 10 ms. The rise of the signal instead tracked the shape of the 200 ps-long pump pulse, showing that the temporal resolution of the E-OPTP spectrometer was sufficient to resolve the photoconductance rise.

An additional consideration in E-OPTP is the accuracy with which the delay time is set. In OPTP experiments, the full range of pump–probe delays is often scanned repetitively. Here, repeated scans of $\Delta T/T$ were found to be shifted in delay time with respect to each other by a maximum of ∼200 ps [Fig. 2(e)]. This is potentially caused by the finite stability of the delay generator's internal clock, which is sensitive to temperature (specified at 2×10^{-6}), creating a drift in delay for long data acquisition times. Such offsets can be readily subtracted before averaging repeated scans.

We now present a method to measure decays over times much longer than the repetition period of the master femtosecond laser (1 ms), impossible with standard OPTP. For any pump–probe measurement, the signal should decay to zero before the next pump pulse excites the sample. Long decays, therefore, require that the interval between pump pulses be increased, readily achieved in E-OPTP by triggering the slave (pump) laser as desired. We used the pulse sequence in Fig. 3, in which E_{on} was sampled at multiple delay times for each pump pulse, and the time needed to measure the reference, E_{off}, was minimized. This "extended mode" method significantly reduced the measurement time. The $\Delta T/T$ for the different sample points was calculated from

$$\left.\frac{\Delta T}{T}\right|_i \equiv \frac{E_{on,i} - E_{off}}{E_{off}} = \frac{(A_i - B_i) - (C - D)}{C - D}, \quad (2)$$

where i indexes the pair of A and B pulses used to calculate $E_{on,i}$ at the sample point i.

The versatility of the extended mode was demonstrated by studying pieces of passivated silicon wafers (Czochralski-grown, 2000 Ω cm p-type, 700 μm thick, 5 ×5 cm^2 across) that underwent a rigorous precleaning procedure before processing.[22] The 20 nm-thick Al_2O_3 layers, formed by 160 cycles of atomic layer deposition (ALD) with O_2 plasma, provided chemical and field-effect surface passivation on both faces of a "double passivated" sample.[23,24] A layer of HfO_2 (100 cycles, corresponding to 10 nm deposited by ALD with O_2 plasma) was deposited on just one side. This made it possible to remove the Al_2O_3 from one side via HF etching while maintaining good passivation of the HfO_2-coated side, creating the "single passivated" sample. The

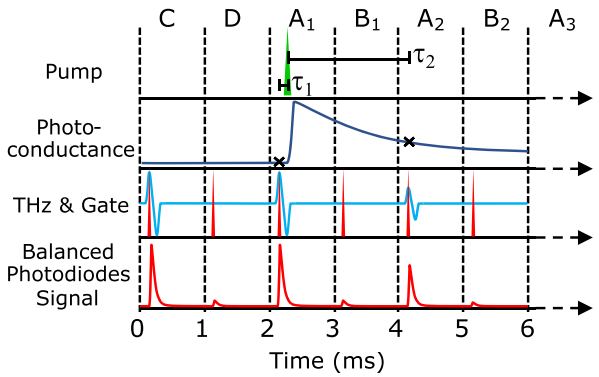

FIG. 3. The extended mode data acquisition scheme, used to record dynamics at delays exceeding the master laser's repetition period (1 ms), with a single pump and multiple THz probes. E_{on} was sampled at multiple pump–probe delay times for each pump pulse (e.g., at τ_1 and $\tau_2 = \tau_1 + 2$ ms), and $\Delta T/T$ was calculated using Eq. (2).

double passivated sample also had one HfO_2 coating, even though no etching step was performed, for consistency with the single passivated sample. Samples were annealed in air at 460 °C in order to activate the passivation.[25,26]

E-OPTP transients using the 450 nm laser are reported in Fig. 4 for the double passivated and single passivated silicon wafers, the latter of which was excited on either the passivated or the etched side. The pump beam's intensity profile had a diameter D4σ = 4 mm at the sample, while the electric field of the THz probe had a Gaussian profile with D4σ = 2.0 mm. The shallow absorption depth [0.4 μm (Ref. 27)] when pumped at 450 nm meant carriers were initially concentrated near the illuminated surface. Hence, the single passivated sample had faster recombination kinetics when excited on the etched side than on the passivated side [Fig. 4(b)].

The high temporal resolution and the range of the E-OPTP enable the rate of diffusion into the depth of the wafer to be studied. While the magnitude of $\Delta T/T$ at a particular pump–probe delay time is not sensitive to the depth dependence of the photoconductivity (a transmission measurement averages over all depths), the $\Delta T/T$ decay rate varies depending on the carriers' depth profile. When illuminated on the passivated side, the transient for the single passivated sample was almost identical to the decay for the double passivated sample for delay times up to 25–30 μs, whereupon $\Delta T/T$ started to decay more quickly for the single passivated sample [Fig. 4(b)]. This is the time required for carriers to diffuse to the unpassivated side of the film, where the surface recombination rate is higher. This assertion is supported by the time-dependent carrier profile calculated using an analytical solution of the 1D ambipolar continuity equation for Si,[28] as reported in Fig. 5(a). Recombination was not included in this model, and for the timescale considered (100 μs) in-plane diffusion was neglected as it proceeds at a slower rate due to its smaller concentration gradient. An appreciable carrier density only arrives at the etched surface (at 700 μm depth) after 20–30 μs, and by around 100 μs, the carriers form a flat distribution with concentration $\simeq 2 \times 10^{13}$ cm^{-3}. This approximately corresponds to the time required to form a stationary distribution, which is supported by the decay curves becoming monoexponential after this time.

The double passivated sample was then used to compare the E-OPTP technique with the established PCD method, the latter of which used a Sinton WCT-120 with a 2 cm spatial resolution (defined by the coil diameter). For PCD, a calibration converted the photoconductance signal into the excess carrier density, Δn, under the assumption that carriers had sufficient time to spread through the depth of the wafer to reach a stationary spatial distribution. The density-dependent effective lifetime,[29] $\tau(\Delta n)$, was calculated from $\tau(\Delta n) = -\Delta n/d(\Delta n)/dt$.[9,30,31] PCD gave $\tau \sim 10$ ms at the highest density $\Delta n = 5 \times 10^{15}$ cm^{-3}, and ~20 ms for lower densities $\Delta n = 10^{15}$ to 10^{13} cm^{-3}. The reduced lifetime at higher densities is consistent with Auger recombination beginning to contribute.[32] In contrast to the PCD lifetimes, for E-OPTP [Fig. 4(a)], an excess $\Delta n \simeq 2 \times 10^{13}$ cm^{-3} was reached following out-of-plane diffusion into the wafer [around 100 μs, Fig. 5(a)], at which time, the double passivated sample had $\tau < 1$ ms, lengthening to ~1.3 ms by the end of the decay.

Therefore, there is a significant disagreement in the lifetime measured by E-OPTP and PCD at comparable densities (10^{13} cm^{-3}). The faster E-OPTP dynamic can be explained by the in-plane diffusion of carriers away from the region probed by the THz pulse, which reduces the carrier density in the probed region, resulting in a decay of the signal. The flux from in-plane diffusion is greatest at early times when the in-plane concentration gradient is greatest and reduces at later times when the gradient is shallower, consistent with $\Delta T/T$ decaying more slowly at late times. This explanation was further supported by analytical solutions to the 2D ambipolar continuity equation, reported in Fig. 5(b) for parameters matching the E-OPTP experiments. The calculated sheet density (the concentration integrated over the

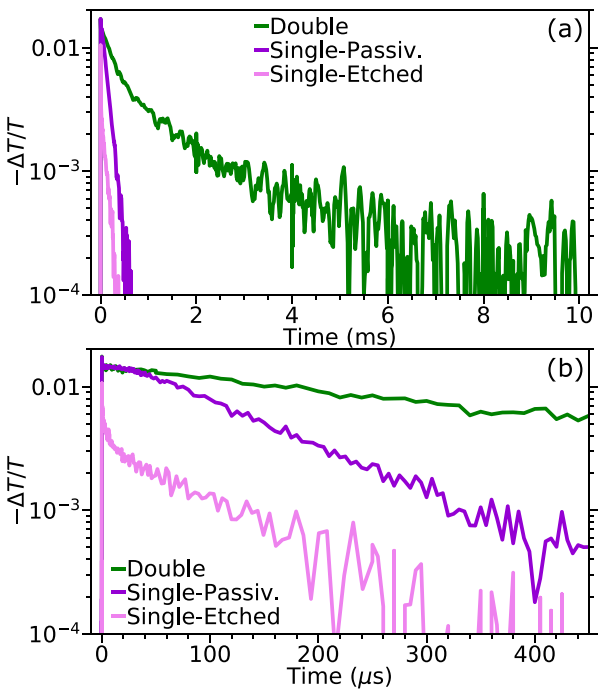

FIG. 4. Photoconductance decays under 450 nm excitation for double-side passivated and single-side passivated Si wafers (illuminated either on its passivated side or on its etched side). (a) Full time window from data acquired in extended mode. (b) Data from (a), but highlighting the first 500 μs.

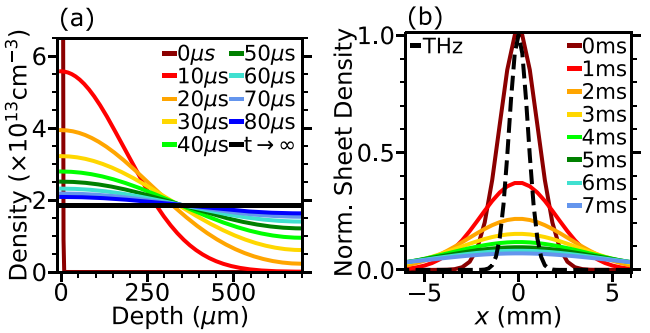

FIG. 5. Carrier density profiles from analytical solutions to the ambipolar continuity equation, ignoring recombination. (a) Excess carrier density, Δn, vs depth at the center of the pump spot, from solving the 1D case (in-plane diffusion was neglected). (b) Profile of the sheet carrier density in the plane of the wafer, from solving the 2D problem. The THz probe (profile in black, dashed line) samples lower density at later times owing to in-plane diffusion.

thickness of the wafer) in the probed region [dashed line in Fig. 5(b)] can be seen to drop on ms timescales (colored lines). Bulk and surface recombination were neglected in these calculations to highlight the effect of diffusion. These measurements demonstrate that the small probe spot size in E-OPTP makes the study of in-plane diffusion effects possible in semiconductors with long diffusion lengths.

In summary, we demonstrated electronically delayed optical pump terahertz probe (E-OPTP) with virtually unlimited delay range, allowing the full photoconductance decay of an optically pumped material to be measured in a non-contact manner with sub-nanosecond resolution. The factors determining temporal resolution were discussed, and an efficient method to sample photoconductance decays longer than the laser repetition period was found. We note that frequency-resolved conductivity spectra can be obtained with this method but are averaged over a small range of pump–probe delays because of the timing jitter. The E-OPTP technique is highly complementary to existing methods to measure photoconductance decays, such as TRMC and PCD, while the superior spatial resolution of the THz probe enables photoconductivity mapping and studies of carrier diffusion.

The data that support the findings of this study are available from the corresponding author upon reasonable request. The authors thank Dr. Igor Khrushchev from Ikeos Research Ltd for providing the MOPA laser and Dr. Tim Niewelt for useful discussions. This work was partially supported by the EPSRC Terabotics Programme (Grant No. EP/V047914/1). E.B.C. and S.L.P. acknowledge funding from the Engineering and Physical Sciences Research Council Doctoral Training Partnership (No. EP/R513374/1).

AUTHOR DECLARATIONS

Conflict of Interest

The authors have no conflicts to disclose.

Author Contributions

Edward Butler-Caddle: Conceptualization (equal); Data curation (lead); Formal analysis (lead); Investigation (lead); Methodology (lead); Software (lead); Validation (lead); Visualization (lead); Writing – original draft (lead); Writing – review & editing (equal). **Nicholas Ewen Grant:** Investigation (equal); Methodology (equal); Supervision (equal); Writing – review & editing (equal). **Sophie L. Pain:** Investigation (equal); Methodology (equal); Writing – review & editing (equal). **John D. Murphy:** Investigation (equal); Methodology (equal); Project administration (equal); Supervision (equal); Writing – review & editing (equal). **K. D. G. Imalka Jayawardena:** Investigation (equal); Methodology (equal); Writing – review & editing (equal). **James Lloyd-Hughes:** Conceptualization (equal); Data curation (equal); Formal analysis (equal); Funding acquisition (lead); Investigation (equal); Methodology (equal); Project administration (lead); Resources (lead); Software (supporting); Supervision (lead); Validation (equal); Visualization (supporting); Writing – original draft (supporting); Writing – review & editing (lead).

DATA AVAILABILITY

The data that support the findings of this study are available from the corresponding authors upon reasonable request.

REFERENCES

[1]R. Ulbricht, E. Hendry, J. Shan, T. F. Heinz, and M. Bonn, Rev. Mod. Phys. **83**, 543 (2011).
[2]J. Lloyd-Hughes and T.-I. Jeon, J. Infrared, Millimeter, Terahertz Waves **33**, 871 (2012).
[3]H. J. Joyce, J. L. Boland, C. L. Davies, S. A. Baig, and M. B. Johnston, Semicond. Sci. Technol. **31**, 103003 (2016).
[4]T. J. Savenije, A. J. Ferguson, N. Kopidakis, and G. Rumbles, J. Phys. Chem. C **117**, 24085 (2013).
[5]M. P. De Haas and J. M. Warman, Chem. Phys. **73**, 35 (1982).
[6]M. Kunst and G. Beck, J. Appl. Phys. **60**, 3558 (1986).
[7]M. Kunst and G. Beck, J. Appl. Phys. **63**, 1093 (1988).
[8]E. Yablonovitch and T. J. Gmitter, Solid State Electron. **35**, 261 (1992).
[9]R. A. Sinton and A. Cuevas, Appl. Phys. Lett. **69**, 2510 (1996).
[10]R. K. Ahrenkiel and S. Johnston, Sol. Energy Mater. Sol. Cells **55**, 59 (1998).
[11]H. Hempel, T. J. Savenjie, M. Stolterfoht, J. Neu, M. Failla, V. C. Paingad, P. Kužel, E. J. Heilweil, J. A. Spies, M. Schleuning, J. Zhao, D. Friedrich, K. Schwarzburg, L. D. Siebbeles, P. Dörflinger, V. Dyakonov, R. Katoh, M. J. Hong, J. G. Labram, M. Monti, E. Butler-Caddle, J. Lloyd-Hughes, M. M. Taheri, J. B. Baxter, T. J. Magnanelli, S. Luo, J. M. Cardon, S. Ardo, and T. Unold, Adv. Energy Mater. **12**, 2102776 (2022).
[12]S. W. Glunz and W. Warta, J. Appl. Phys. **77**, 3243 (1995).
[13]J. S. Blakemore, *Semiconductor Statistics*, International Series of Monographs on Semiconductors, edited by J. S. Blakemore (Pergamon Press, Pergamon, 1962), pp. 319–342.
[14]J. Neu and M. Rahm, Opt. Express **23**, 12900 (2015).
[15]R. Lin, K. Xiao, Z. Qin, Q. Han, C. Zhang, M. Wei, M. I. Saidaminov, Y. Gao, J. Xu, M. Xiao, A. Li, J. Zhu, E. H. Sargent, and H. Tan, Nat. Energy **4**, 864 (2019).
[16]T. Seifert, S. Jaiswal, U. Martens, J. Hannegan, L. Braun, P. Maldonado, F. Freimuth, A. Kronenberg, J. Henrizi, I. Radu, E. Beaurepaire, Y. Mokrousov, P. M. Oppeneer, M. Jourdan, G. Jakob, D. Turchinovich, L. M. Hayden, M. Wolf, M. Münzenberg, M. Kläui, and T. Kampfrath, Nat. Photonics **10**, 483 (2016).
[17]M. G. Burdanova, A. P. Tsapenko, D. A. Satco, R. Kashtiban, C. D. Mosley, M. Monti, M. Staniforth, J. Sloan, Y. G. Gladush, A. G. Nasibulin, and J. Lloyd-Hughes, ACS Photonics **6**, 1058 (2019).
[18]M. Saliba, T. Matsui, J. Y. Seo, K. Domanski, J. P. Correa-Baena, M. K. Nazeeruddin, S. M. Zakeeruddin, W. Tress, A. Abate, A. Hagfeldt, and M. Grätzel, Energy Environ. Sci. **9**, 1989 (2016).
[19]R. M. Bandara, K. D. Jayawardena, S. O. Adeyemo, S. J. Hinder, J. A. Smith, H. M. Thirimanne, N. C. Wong, F. M. Amin, B. G. Freestone, A. J. Parnell, D. G. Lidzey, H. J. Joyce, R. A. Sporea, and S. R. Silva, J. Mater. Chem. C **7**, 8389 (2019).
[20]E. Gaubas and J. Vanhellemont, Appl. Phys. Lett. **89**, 142106 (2006).
[21]A. Leitenstorfer, S. Hunsche, J. Shah, M. C. Nuss, and W. H. Knox, Appl. Phys. Lett. **74**, 1516 (1999).
[22]N. E. Grant, T. Niewelt, N. R. Wilson, E. C. Wheeler-Jones, J. Bullock, M. Al-Amin, M. C. Schubert, A. C. van Veen, A. Javey, and J. D. Murphy, IEEE J. Photovoltaics **7**, 1574 (2017).
[23]G. Dingemans and W. M. M. Kessels, J. Vac. Sci. Technol., A **30**, 040802 (2012).
[24]L. E. Black, *New Perspectives on Surface Passivation: Understanding the Si-Al2O3 Interface* (Springer, 2016), pp. 181–204.
[25]N. E. Grant, A. I. Pointon, R. Jefferies, D. Hiller, Y. Han, R. Beanland, M. Walker, and J. D. Murphy, Nanoscale **12**, 17332 (2020).
[26]S. L. Pain, E. Khorani, T. Niewelt, A. Wratten, G. J. Paez Fajardo, B. P. Winfield, R. S. Bonilla, M. Walker, L. F. J. Piper, N. E. Grant, and J. D. Murphy, Adv. Mater. Interfaces **9**, 2201339 (2022).
[27]M. A. Green, Sol. Energy Mater. Sol. Cells **92**, 1305 (2008).
[28]Combining the electron and hole continuity equations and the Poisson equation into a single ambipolar continuity equation assumes that there is negligible net trapping of either electrons or holes, meaning that their populations are always equal, and they share the same lifetime. An analytical solution can then be found if this common lifetime is independent of density (e.g., by separation of variables). Recombination and transport were assumed to be negligible

during the pump pulse, so the initial distribution was given by the measured generation profile.
[29]The "effective" lifetime incorporates the rates from both bulk and surface recombination and, hence, depends on the carrier profile with depth.
[30]D. K. Schroder, *Semiconductor Material and Device Characterization* (John Wiley & Sons, Ltd, 2005), pp. 389–464.
[31]A. Cuevas, D. Macdonald, and R. A. Sinton, *McEvoy's Handbook of Photovoltaics*, 3rd ed., edited by S. A. Kalogirou (Academic Press, 2018), pp. 1119–1154.
[32]T. Niewelt, B. Steinhauser, A. Richter, B. Veith-Wolf, A. Fell, B. Hammann, N. E. Grant, L. Black, J. Tan, A. Youssef, J. D. Murphy, J. Schmidt, M. C. Schubert, and S. W. Glunz, Sol. Energy Mater. Sol. Cells **235**, 111467 (2022).